Extra-polar cloud feedbacks as a driver of Arctic amplification

Qiuxian Li[a], Kyle C. Armour[c,d], Wei Cheng[b], LuAnne Thompson[c], Jian Lu[f], Jiaxu Zhang[a,b], Bryce E. Harrop[e], Oluwayemi A. Garuba[e], Yiyong Luo[f]

[a] *Cooperative Institute for Climate, Ocean, and Ecosystem Studies, University of Washington, Seattle, WA*

[b] *NOAA Pacific Marine and Environmental Laboratory, Seattle, WA*

[c] *School of Oceanography, University of Washington, Seattle, WA*

[d] *Department of Atmospheric and Climate Science, University of Washington, Seattle, WA*

[e] *Atmospheric, Climate and Earth Science Division, Pacific Northwest National Laboratory, Richland, WA*

[f] *Frontiers Science Center for Deep Ocean Multispheres and Earth System, Physical Oceanography Laboratory, and College of Oceanic and Atmospheric Sciences, Ocean University of China, Qingdao, China*

Corresponding author: Qiuxian Li, qxli@uw.edu

Peer review status: This is a non-peer-reviewed preprint submitted to EarthArXiv

Submitted to *Journal of Climate*

ABSTRACT

The role of cloud feedbacks in Arctic amplification (AA) of anthropogenic warming remains unclear. Traditional feedback analysis diagnoses the net cloud feedback as strongly positive in the tropics but either weak or negative in the Arctic, suggesting that AA would be amplified if cloud feedbacks were suppressed. However, in cloud-locking experiments using the slab ocean version of the Energy Exascale Earth System Model (E3SM), we find that suppressing cloud feedbacks results in a substantial decrease in AA under greenhouse gas forcing. We show that the increase in AA from cloud feedbacks arises from two main mechanisms: 1) the additional energy contributed by positive cloud feedbacks in the tropics leads to increased poleward moist atmospheric heat transport (AHT) which then amplifies Arctic warming; 2) the additional Arctic warming is amplified by positive non-cloud feedbacks in the region, altogether making extra-polar cloud feedbacks amplify AA. We also find that cloud changes can modify the strength of non-cloud feedback, which has a small effect on Arctic warming. We further validate the role of cloud feedbacks in AA using a moist energy balance model, which demonstrates that interactions of cloud feedbacks with moist AHT and other positive feedbacks dominate their influence on the pattern of surface warming. Moreover, the predicted AA shows little variation when the effect of cloud feedbacks on non-cloud feedback is considered. These results demonstrate that traditional attributions of AA, based on local feedback analysis, overlook key interactions between extra-polar cloud changes, poleward AHT, and non-cloud feedbacks in the Arctic.

1. Introduction

Analysis of observations (Serreze et al. 2009; Screen and Simmonds 2010; Collins et al. 2013) and climate model simulations (Manabe and Stouffer 1980; Holland and Bitz 2003; Taylor et al. 2021) show that the Arctic experiences greater surface warming than other regions under increased greenhouse gas forcing – a phenomenon known as Arctic amplification (AA). Many mechanisms have been proposed to explain this amplified warming in the Arctic (e.g., Pithan and Mauritsen 2014; Singh et al. 2017; Stuecker et al. 2018; Hahn et al. 2021; Feldl and Merlis 2021), involving both local processes and changes in poleward energy transports. Currently there is no consensus on the main driver of AA as many different processes have been proposed to play a role (e.g., Forster et al. 2021).

In addition, the uncertainty in Arctic warming projections exceeds that of any other region, in part owing to challenges in accurately quantifying cloud feedbacks (Bonan et al. 2018; Zelinka et al. 2020; Hahn et al. 2021; Previdi et al. 2021). Significant uncertainties persist regarding cloud properties and their radiative effects in polar regions (Randall et al. 1998; Shupe and Intrieri 2004; Kay and Gettelman 2009; Boeke and Taylor 2016; Kato et al. 2018). Given that the poles are the regions most sensitive to greenhouse gas forcing (Boeke and Taylor 2018; Constable et al. 2022; González-Herrero et al. 2024), it is crucial to determine how clouds respond to climate change and whether these changes will enhance or dampen warming in the Arctic and consequently AA.

Previous studies have employed various methods to assess the impact of cloud feedbacks on AA. For instance, several studies (Pithan and Maurisen 2014; Goosse et al. 2018; Hahn et al. 2021) used a radiative feedback analysis and found that cloud feedbacks slightly reduce AA in climate models. They argued that this occurs because the net cloud feedback is strongly positive in the tropics but either weak or negative in the Arctic. In contrast, Vavrus (2004) compared two simulations—one with and one without changes in cloud fraction under 2×CO_2 forcing in an atmosphere–slab ocean model—and found that cloud feedbacks amplify AA. Meanwhile, Middlemas et al. (2020) used a cloud locking method in the coupled Community Earth System Model (CESM) and found that the influence of cloud feedbacks increased both global and Arctic warming by approximately the same amount, around 25%, thus concluding that cloud feedbacks did not substantially contribute to AA. These findings show the complexity and ongoing uncertainty about the role of cloud feedbacks in AA.

The discrepancies between the conclusions of these studies can be partially attributed to the use of different methods to assess the contribution of cloud feedbacks. For example, traditional feedback analysis methods, such as that employed by Hahn et al. (2021), use a linear diagnostic framework and thus do not capture the interactions between cloud feedbacks, non-cloud feedbacks, and atmospheric heat transport (AHT). Cloud locking methods offer a distinct advantage over this traditional feedback analysis in that cloud locking not only eliminates cloud feedbacks but also interrupts their interactions with non-cloud feedbacks and AHT (Vavrus 2004; Mauritsen et al. 2013; Grise et al. 2019; Middlemas et al. 2019; Harrop et al. 2024). Since local feedbacks influence meridional temperature gradients and local radiation, they must also influence AHT (e.g., Hwang and Frierson 2010; Hwang et al. 2011; Armour et al. 2019). Thus, the coupling between AHT and local feedbacks is important for understanding AA

(Huang et al. 2017). The cloud locking approach provides a comprehensive assessment of the role of cloud feedbacks in AA, but a key question is how to reconcile its findings with traditional feedback analyses.

In this study, we examine the role of cloud feedbacks in AA using cloud locking techniques in both a comprehensive global climate model (GCM) and a moist energy balance model (MEBM) that includes the interactions between feedbacks and AHT. We also apply traditional feedback analyses, and compare the findings between the two approaches to demonstrate that extra-polar cloud feedbacks (i.e., cloud feedbacks outside the Arctic) play a key role in driving AA through their interactions with AHT and non-cloud feedbacks in the Arctic.

2. Model and experiments

The comprehensive GCM we employ here is the Slab Ocean Model (SOM) version of the Energy Exascale Earth System Model version 2 (E3SMv2-SOM; Golaz et al. 2022; Garuba et al. 2024). E3SMv2 is a state-of-the-art climate model that includes the E3SM Atmosphere Model (EAM; Rasch et al. 2019), the E3SM Land Model (ELM), the Model for Prediction Across Scales ocean model (MPAS-O), and the MPAS sea ice model (MPAS-SI) (Petersen et al. 2019). E3SMv2-SOM has a 110 km atmosphere with 72 layers, 165 km land, 0.5° river routing model, and an ocean and sea ice with mesh spacing varying between 60 km in the mid-latitudes and 30 km at the equator and poles (Golaz et al. 2022). In the E3SMv2-SOM configuration, the dynamic MPAS-O model component is replaced with the SOM component, and other model components are identical with the E3SMv2. E3SMv2-SOM effectively reproduces the baseline climate of the fully coupled simulations of E3SMv2 experiments (Garuba et al. 2024), including temperature, precipitation, and sea ice concentration.

We perform an initial pre-industrial control simulation of the E3SMv2-SOM using the ocean heat transport convergence (referred to as q-flux) and mixed layer depth (MLD) obtained from a fully coupled, high-resolution simulation of an earlier version of E3SM (E3SMv1-HR; Caldwell et al. 2019). Since the ocean heat transport is overall too strong in that simulation, applying the q-flux directly within E3SMv2-SOM results in a warmer mean climate compared to the HadISST climatology of 1870-1900 (17.4°C vs. 13.7°C; Rayner et al. 2003). To address this, we conduct a set of sensitivity tests and find that reducing the q-flux values at each grid point by 40% significantly reduces the warm bias. We then use an iterative equilibration approach (Wang et al. 2019) to fine-tune the q-flux, resulting in a sea surface temperature (SST) climatology that closely matches the HadISST climatology (Rayner et al., 2003). The E3SMv2-SOM simulation using this fine-tuned q-flux defines the pre-industrial control climatology for this study.

Branched from this pre-industrial control simulation, we perform two pairs of E3SMv2-SOM simulations (Table 1) to evaluate the role of clouds in the climate response to greenhouse gas forcing. We first integrate a pair of simulations with pre-industrial and quadrupled CO_2 levels (A1 and A4; Table 1). We refer to this pair as “cloud-active” simulations because clouds are allowed to actively evolve with and influence the climate state. We integrate a second pair of simulations that are similar to the first pair, except that the cloud optical properties are replaced by pre-industrial values taken from the pre-industrial control simulation everywhere on the globe and at all vertical levels (L1 and L4; Table 1). Specifically, the cloud optical properties from the last three years of the pre-industrial control simulation are saved at an hourly frequency and are prescribed to L1 and L4 on an hourly basis during radiative transfer calculations. This “cloud locking” technique disables cloud radiative feedbacks (see Harrop et al. 2024 for more details about the method), and thus we refer to this pair as “cloud-locked” simulations. The role of cloud feedbacks in the climate response to CO_2 forcing can be quantified by comparing the response of simulations with active (A4 minus A1) and locked clouds (L4 minus L1). All the simulations are 50 years in length, and we use the last 30 years for analyses.

Table 1: Model experiments

Name		**Length (Yrs)**	**CO_2 level**	**Cloud condition**
Cloud-active	A1	50	$1\times CO_2$	Active
	A4	50	$4\times CO_2$	Active
Cloud-locked	L1	50	$1\times CO_2$	Locked to A1
	L4	50	$4\times CO_2$	Locked to A1

3. Results

a. Surface Temperature Response

In response to CO_2 quadrupling (4×CO_2), the surface temperature increases everywhere with amplified warming at both poles in both cloud-active and cloud-locked simulations (Fig. 1a). The global mean surface warming in the cloud-locked simulation (4.81 K) is only half as large as that in the cloud-active simulation (8.72 K[1]). While the magnitude of surface warming is reduced everywhere when clouds are locked, the most substantial warming reduction occurs in the Arctic where cloud locking reduces warming by around 11 K (Figs. 1a-c). The amplification index (defined as zonal-mean surface warming normalized by global-mean surface warming) also shows that the impact of interactive cloud changes is most significant in the Arctic, where AA (defined as the ratio of surface warming average north of 60°N to global surface warming) increases from 1.72 to 1.98 (an increase of ~15%) when cloud feedbacks are included (black line in Fig. 1d). If an alternative definition of AA is applied, defined as the ratio of surface warming between the Arctic (60°N-90°N) and the tropics (30°S-30°N), the AA increase from 2.17 to 2.58 when cloud feedbacks are included (an increase of ~19%). These results are consistent with those of Vavrus (2004) who also found that cloud feedbacks enhance AA.

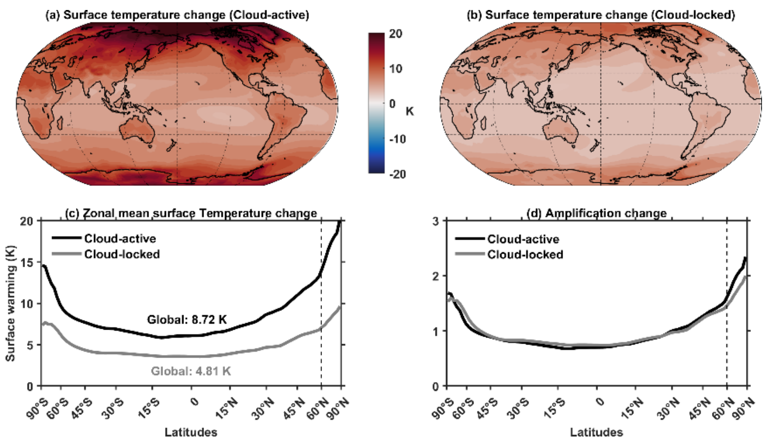

Fig. 1. Changes of surface temperature (K) in response to 4×CO_2 in (a) cloud-active and (b) cloud-locked simulations. (c) Changes of zonal mean surface temperature in cloud-active (black) and cloud-locked (gray) simulations, with area weighted global mean indicated by the numbers. (d) Changes of amplification (zonal-mean surface warming normalized by global-mean surface warming) in cloud-active (black) and cloud-locked (gray) simulations. Latitude axes in (c) and (d) are area weighted.

[1] The Equilibrium Climate Sensitivity (ECS) of the E3SMv2-SOM estimated in this study (4.36 K) differs slightly from the value reported by Garuba et al. (2024) for E3SMv2-SOM (4.5 K), likely due to slight differences in the prescribed q-flux.

b. Cloud Feedback diagnoses and correction

To examine how the various radiative feedbacks in E3SM contribute to AA, we use a radiative kernel analysis. The radiative kernels used here are calculated from CESM1-CAM5 (Pendergrass et al. 2018). We also test the results of using ERA kernel (Huang et al. 2017) and the results are qualitatively similar. We find that, compared to the surface albedo kernel in Huang et al. (2017), the surface albedo kernel derived from CESM1-CAM5 agrees better with the one estimated from the climatological radiative fields in E3SM using an idealized isotropic radiation model (Donohoe et al. 2020a) applied in the Arctic region (Figure A1), indicating that the CESM1-CAM5 kernels are more appropriate for use in calculating the surface-albedo feedback in the E3SM. Additionally, the errors in the clear-sky kernel decomposition are smaller than 15% of the magnitude of both the clear-sky longwave and shortwave (Figure A2) and satisfy the clear-sky linearity test (Caldwell et al. 2016). In addition, we use an adjusted Cloud Radiative Effect (CRE) method to calculate the cloud feedbacks (Soden et al. 2008; Shell et al. 2008):

$$\delta R_c = \Delta C_{RE} + (K_T^0 - K_T)\Delta T + (K_W^0 - K_W)\Delta W + (K_a^0 - K_a)\Delta a + (\mathrm{ERF}^0 - \mathrm{ERF}) \quad (1)$$

where δR_c is the cloud feedbacks; ΔC_{RE} is the CRE, defined as the difference in the top-of-atmosphere radiation between all-sky and clear-sky conditions (e.g., Charlock and Ramanathan 1985); K_x are the all-sky kernels (where x=T, W, a, corresponding to the temperature, water vapor, and albedo kernels, respectively), defined as the ratio of the all-sky radiative flux change at the top-of-atmosphere due to specific variables to the perturbation in those variables; ERF is the effective radiative forcing for 4×CO_2 in all-sky conditions; K_x^0 and ERF^0 represents the correspond values in clear-sky conditions; Δx represent the changes in the climate variables in response to greenhouse gas forcing in E3SM. The last four terms on the right-hand side of Eq. (1) represent the effects of cloud masking on non-cloud feedbacks (i.e., temperature, water vapor, and surface albedo) and radiative forcing (i.e., ERF), which are added to the change in CRE to estimate cloud feedbacks. We derive the ERF of 4×CO_2 from fixed-SST experiments using E3SMv2 (Qin et al. 2024).

Figure 2 shows the local cloud feedbacks diagnosed according to equation (1) (i.e., the local top-of-atmosphere radiation response due to cloud changes per degree of local surface temperature change) in both the E3SM cloud-active and cloud-locked simulations. In the cloud-active simulation, the net cloud feedback is positive in the tropics but negative in the Arctic, with a global mean of 0.57 W m^{-2} K^{-1}. This feedback analysis suggests that the net cloud feedback should, on its own, act to reduce AA, which conflicts with the simulated increase in AA when cloud feedbacks are active (Fig. 1d). A possible reason for this conflict is that cloud feedbacks affect surface temperature not only through directly influencing top-of-atmosphere radiation but also by influencing AHT and interacting with other, non-cloud feedbacks. We will discuss these processes in detail in the following subsections.

We can also use the cloud-locked simulations to assess the accuracy of the adjusted CRE method (Eq. (1)). By construction, the diagnosed cloud feedback in the cloud-locked simulation should be zero everywhere, with zero global mean. However, contrary to this expectation, we find that it is slightly negative everywhere, with a global mean of -0.33 W m^{-2} K^{-1}. The negative values stem from SW cloud effects in the polar regions and LW cloud effects in extra-polar regions (Fig. 2b). This suggests that the cloud masking correction still leaves an error margin in diagnosing cloud feedbacks with radiative kernels.

While a full accounting of the cause of this kernel-derived cloud feedback error is beyond the scope of this study, the result in Fig. 2b suggests a path for its correction. Assuming that the error is the same in both the cloud-active and cloud-locked simulations, we can correct the cloud feedback in each simulation by subtracting off this term (represented by the negative adjusted CRE in cloud-locked simulation shown in Figure 2b); we refer to these as "corrected cloud feedbacks". After applying this correction, we obtain zero cloud feedbacks in the cloud-locked simulation (by construction) and more-positive cloud feedbacks in the cloud-active simulation. The corrected cloud feedback in E3SM is broadly positive except in the tropics and weakly positive in the Arctic, with a global mean of 0.90 W m^{-2} K^{-1} (Figure 2c). The global mean value and the overall patterns of the corrected cloud feedback closely matches those derived using the Cloud Radiative Kernel (CRK) method (Zelinka et al. 2012; Fig. A3), which more effectively captures key aspects of cloud feedback, particularly in the Arctic, as it is less affected by surface albedo changes (Coulbury and Tan 2024). Hence, the agreement between the corrected cloud feedbacks and those derived from the CRK method increases our confidence in this correction method. In the following analyses, 'cloud feedback' refers to the corrected cloud feedback.

Next, we quantify the cloud and other feedbacks' contributions to AA following the commonly-used warming contribution analysis (Pithan and Mauritsen 2014; Goosse et al. 2018; Hahn et al. 2021).

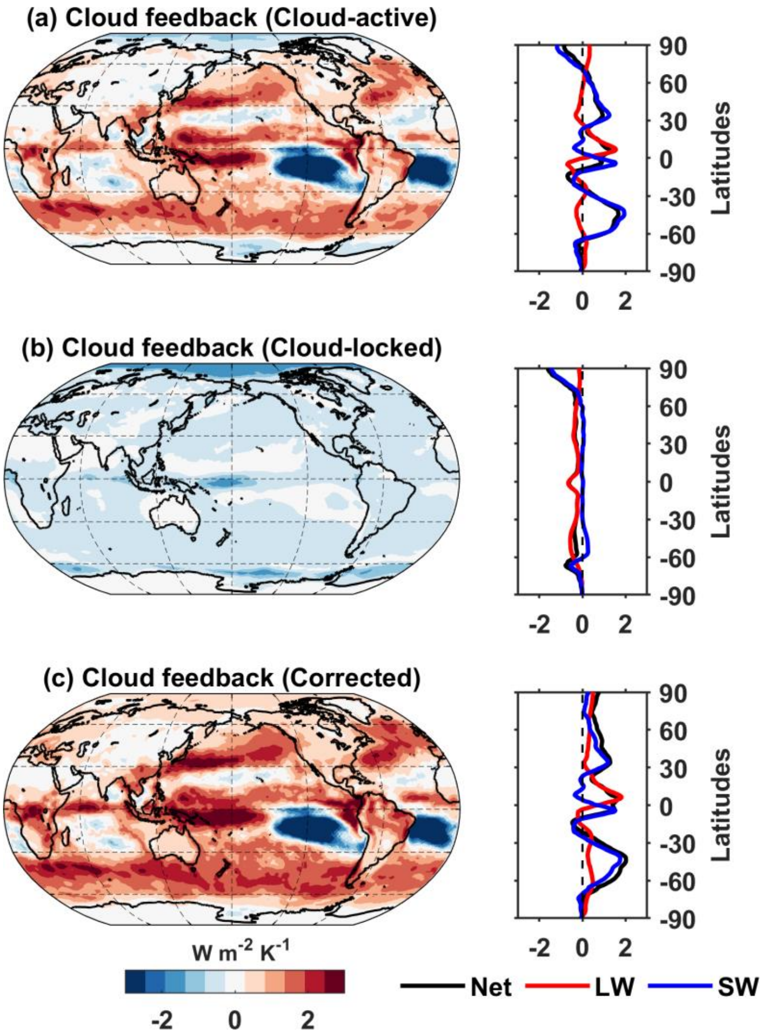

Fig. 2. Spatial patterns of local cloud feedbacks within E3SM (a) cloud-active and (b) cloud-locked simulations. (c) is the corrected cloud feedbacks in cloud-active simulation. The right-side panels are the zonal mean net cloud feedback (black) and its longwave (LW, red) and shortwave (SW, blue) components.

c. Warming Contribution

The warming contribution analysis provides an estimate of the degree to which each feedback process and AHT convergence contributes to regional warming (and thus to AA). By comparing the warming contributions of non-cloud feedbacks and AHT between the cloud-active and cloud-locked simulations in E3SM, we can assess the indirect impacts of interactive clouds on temperature response.

Following Hanh et al. (2021), the change in surface temperature (ΔT) can be attributed to contributions from ERF, the Planck response (λ_p'), radiative feedbacks (λ_x), the anomalies in atmospheric heat transport convergence ($-\Delta\nabla \cdot \mathrm{AHT}$), and a residual term ($res$):

$$\Delta T = -\frac{\mathrm{ERF}}{\overline{\lambda_p}} - \frac{\lambda_p' \Delta T}{\overline{\lambda_p}} - \frac{\sum_{x \neq p} \lambda_x \Delta T}{\overline{\lambda_p}} - \frac{\Delta \nabla \cdot \mathrm{AHT}}{\overline{\lambda_p}} - \frac{res}{\overline{\lambda_p}} \tag{2}$$

where $\overline{\lambda_p}$ is the global- and annual-mean Planck feedback; λ_p' is the location deviation in the Planck feedback from $\overline{\lambda_p}$; and λ_x represents other radiative feedback parameters (including water vapor, lapse-rate, surface albedo, and cloud feedbacks), the cloud feedbacks are calculated following section 3b, and all the non-cloud feedbacks are calculated by multiplying the climate variable's response to 4xCO_2 (Δx) by the corresponding radiative kernel (K_x) and then normalizing by the local surface temperature response:

$$\lambda_x(r) = \frac{K_x(r)\Delta x}{\Delta T(r)} \tag{3}$$

where $r = (latitude, longitude)$. Again, we use the CESM1-CAM5 (Pendergrass et al. 2018) kernel to calculate the feedbacks and ERF derived from the E3SM fixed SST experiments (Qin et al. 2024). The change in atmospheric heat transport convergence, $\nabla \cdot \mathrm{AHT}$, can be partitioned into moist ($\nabla \cdot \mathrm{AHT_m}$) and dry ($\nabla \cdot \mathrm{AHT_d}$) components (Donohoe et al. 2020b; Hahn et al. 2021). By comparing the warming amplitudes and their contributing components between the Arctic (60°N-90°N) and the tropics (30°S-30°N), we can identify the drivers of AA.

The results from the cloud-active simulation are consistent with previous studies (Pithan and Mauritsen 2014; Goosse et al. 2018; Hahn et al. 2021), showing that the key contributors to AA are the lapse-rate, surface-albedo, and Planck feedbacks, as well as moist AHT convergence (see the four dots in the upper left of Fig. 3a). Dry AHT convergence has a negative contribution to AA that largely compensates the contribution of moist AHT convergence, resulting in a near-zero net contribution from total AHT convergence. Before correcting the cloud feedbacks following the method described in 2.1b, both the cloud feedbacks and the residual term show a relatively weak negative contribution to AA (cyan and yellow circles in Fig. 3a), consistent with Hahn et al. (2021). However, the corrected cloud feedback, in combination with temperature response, contributes slightly positively to AA (cyan dot in Fig. 3a). To be specific, although positive cloud feedbacks (λ_c, Fig. 2c) are stronger in the tropics than in the Arctic, the surface warming (ΔT, Fig. 1c) is greater in the Arctic than in the tropics. This difference in surface warming overcomes the difference in the feedback parameter, resulting in the warming contribution of cloud feedbacks ($\lambda_c \Delta T$) being greater in the Arctic. In addition, since the total temperature response remains unchanged, correcting the cloud feedback introduces a change in the residual term. The corrected residual term, which includes all unidentified and nonlinear processes, now exhibits a stronger cooling effect in the Arctic (yellow dot in Fig. 3a). The cooling effect of the residual term in the Arctic is consistent with the negative radiation change caused by the nonlinear effect of surface-albedo feedback and cloud-albedo coupling effect identified in previous studies (Huang et al. 2021).

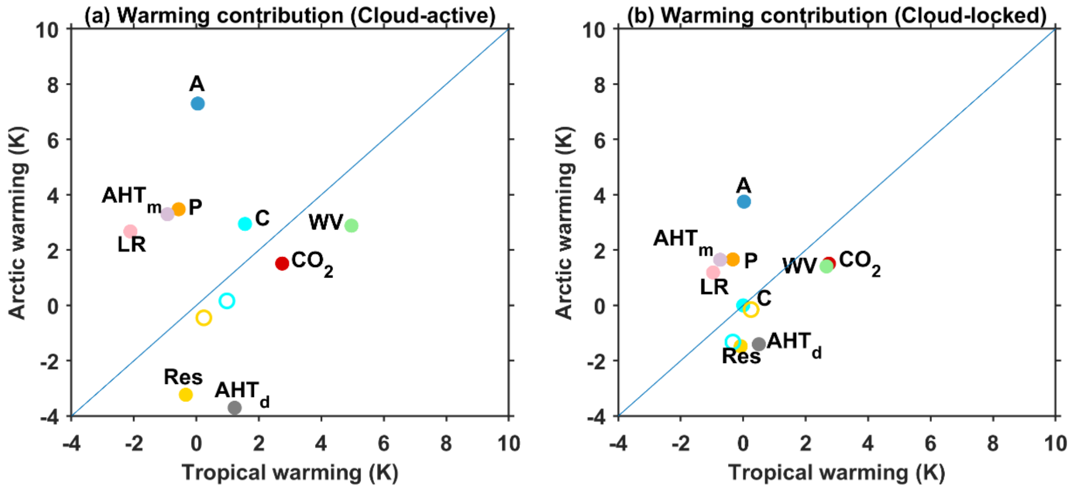

Fig. 3 Contributions of each local feedback and atmospheric forcing to warming (K) in response to abrupt CO_2 quadrupling for the tropics relative to the Arctic in E3SM (a) cloud-active and (b) cloud-locked simulations. Warming contributions are shown for the lapse-rate (LR), surface-albedo (A), water-vapor (WV), Planck (P) and cloud (C) feedback, the effective radiative forcing (CO_2), change in moist AHT convergence (AHT_m); change in dry AHT convergence (AHT_d) and residual term (Res). The open circle shows the result before cloud feedback correction.

The cloud-locked simulation shows that when clouds are suppressed, the contribution of the (corrected) cloud feedback to AA is reduced to zero, as expected. Moreover, the contributions of all other feedbacks and processes also change significantly in response to cloud locking (Fig. 3b). Specifically, the contributions of lapse-rate, surface-albedo, Planck feedbacks, and moist AHT convergence to AA all decrease in the cloud-locked simulation (compare Fig. 3b with Fig. 3a). This suggests that cloud feedbacks influence surface temperature not only directly by changing local top-of-atmosphere radiation, but also indirectly by affecting AHT and the warming contributions of other, non-cloud feedbacks. According to Eq. (2), the warming contribution of a specific feedback is determined by both the feedback parameter (λ_x) and the local temperature response (ΔT). Therefore, changes in both the local feedback parameter and the local temperature response can influence the magnitude of the warming contribution from that feedback. To determine whether the reduced contribution of lapse-rate, surface-albedo, and Planck feedbacks to AA when clouds are locked is due to changes in the local feedback parameters or simply to reduced local warming, we next examine how these feedback parameters respond to locked clouds.

d. Local Feedbacks

By applying our feedback analysis to both cloud-active and cloud-locked simulations, we evaluate how cloud responses influence non-cloud feedbacks. Figure 4 compares the zonal-mean local feedback parameters between the cloud-active and cloud-locked simulations. The results indicate that suppressing cloud responses modifies the strength of local non-cloud feedbacks, making the water-vapor feedback less positive and the lapse-rate feedback less negative in the tropics. The largest changes in water-vapor feedback occur in the Northern Hemisphere, while those of the lapse-rate feedback occur in the Southern Hemisphere. At the same time, the surface albedo feedback becomes more positive in the polar regions when clouds are locked (Fig. 4c). The reduced water-vapor and lapse-rate feedbacks when clouds are locked are consistent with findings from previous studies (Mauritsen et al. 2013; Middlemas et al. 2020). The global-mean changes in water-vapor and lapse-rate feedback parameters largely cancel each other out. Thus, the influence of cloud changes on non-cloud feedbacks is primarily manifested as an enhancement of local surface-albedo feedbacks in the polar regions when clouds are locked.

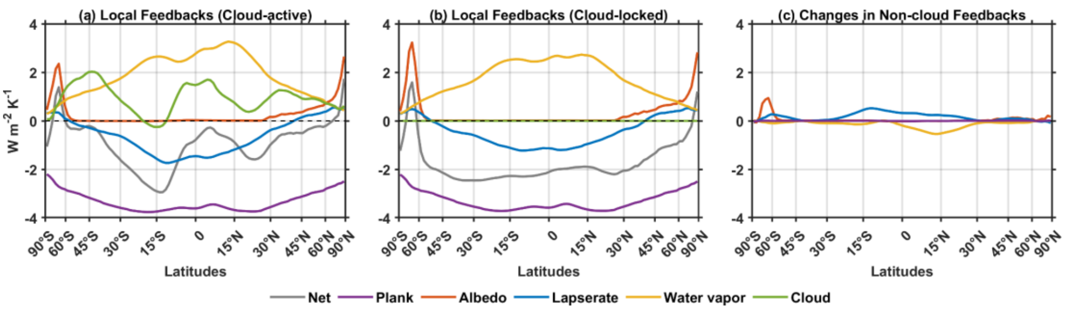

Fig. 4 Zonal-mean local feedbacks within E3SM (a) cloud-active and (b) cloud-locked simulations. (c) Changes in zonal-mean local non-cloud feedbacks caused by cloud locking. Latitude axes are presented in equal-area increments in all figures.

To investigate the mechanisms by which cloud responses drive changes in water vapor and lapse-rate feedbacks, we compare the vertical structure of temperature and specific humidity responses between the cloud-active and cloud-locked simulations (Fig. 5). It is important to note that, to be consistent with local feedback diagnoses, we normalize the vertical temperature and humidity responses by the local surface temperature response. We find that locking clouds weakens tropical upper tropospheric warming per degree of local surface warming (Fig. 5c), resulting in weaker negative lapse-rate feedbacks (Fig. 4c). This is consistent with Voigt and Shaw (2015), who found that radiative changes due to clouds warm the upper troposphere. Correspondingly, reduced tropospheric warming leads to a smaller increase in humidity (Fig. 5f), consistent with the decrease in water-vapor feedbacks in the cloud-locked simulation (Fig. 4c). For the surface-albedo feedback, we examine the sea ice response in both the cloud-active and cloud-locked experiments. The cloud-locked simulation exhibits greater change in sea ice concentration per degree of local surface warming (Fig. 6), consistent with the stronger surface-albedo feedback parameters in polar regions. This enhanced ice loss may result from nonlinear interactions between sea ice and cloud changes, as cloud-albedo coupling can produce a negative radiative response in polar regions (Huang et al. 2021), which is absent in the cloud-locked simulation.

Overall, the changes in local non-cloud feedbacks caused by cloud locking are small (Fig. 4c). The enhanced surface-albedo feedback in the Arctic region caused by cloud locking acts to weakly compensate the substantial reduction in Arctic warming in the cloud-locked simulation (Fig. 1c), while lapse-rate and water-vapor feedbacks play little role. It is thus the changes in local temperature response (acting on a near-constant set of local feedbacks) that drive the differences in the warming contributions from non-cloud feedbacks to AA between cloud-active and cloud-locked simulations. Since local cloud feedbacks are strongly positive in the tropics but only weakly positive in the Arctic, it is likely that tropical cloud feedbacks influence Arctic warming through changes in AHT. Therefore, in the following section, we examine the impact of cloud locking on the response of AHT, considering both its moist and dry components.

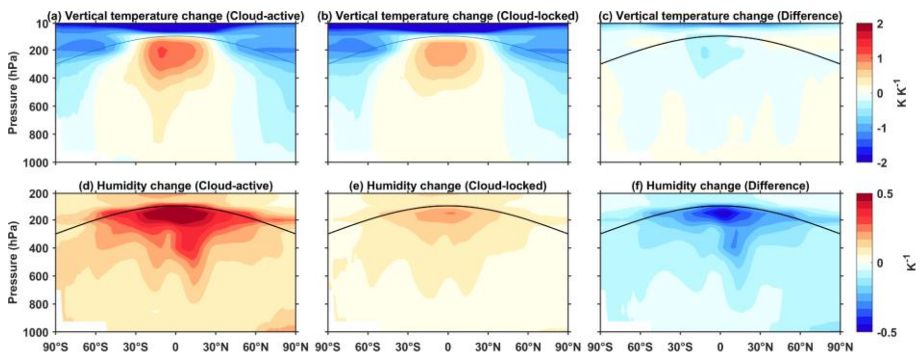

Fig. 5 Changes in zonal-mean vertical temperature structure per degree local surface temperature change (K K^{-1}) within E3SM (a) cloud-active simulation, (b) cloud-locked simulation and (c) their difference. (d)-(e) like (a)-(c) but for the change in the zonal-mean logarithm of the specific humidity per degree local surface temperature change (K^{-1}).

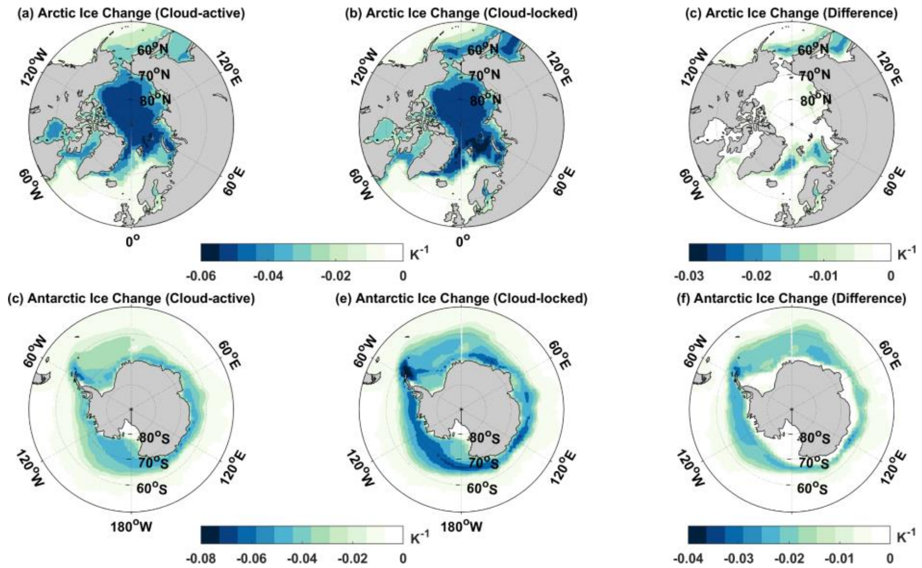

Fig. 6 Changes in Arctic sea ice concentration per degree local surface temperature change (K^{-1}) within E3SM (a) cloud-active simulation, (b) cloud-locked simulation and (c) their difference. (d)-(e) is the same as (a)-(c) for the Antarctic.

e. Atmospheric Heat Transport

Following Donohoe et al. (2020b), the total AHT and moist AHT are calculated as the meridional integral of the net atmospheric heat flux (sum of energy fluxes at the surface and top-of-atmosphere) and atmospheric latent heat flux (energy fluxes associated with surface evaporation minus precipitation), respectively. The dry component of AHT is then derived as the difference between the total AHT and the moist component.

There is an increase in northward moist AHT into the Arctic in both the cloud-active and cloud-locked simulations under $4\times CO_2$ (blue lines in Figs. 7a and 7b), consistent with the positive contributions of moist AHT to AA (purple dot in Fig. 3). The enhanced Arctic warming weakens the equator-to-pole temperature gradient leading to a reduction in atmospheric dry static energy transport that can exceed the increase in atmospheric latent heat transport, resulting in a small change in the total AHT across 60°N in both simulations (black lines in Figs. 7a and 7b). This suggests that the moist AHT acts as a driver of AA, whereas the dry AHT adjusts in response to AA (Armour et al. 2019; Hahn et al. 2021). Hence, we mainly focus on how cloud feedbacks modify AA through their impact on the response of moist AHT.

Poleward moist AHT anomalies is substantially larger when clouds are active (compare blue line in Figs. 7a and 7b), as positive cloud feedbacks in the tropics and mid-latitudes act to increase warming locally, enhancing the meridional energy and moisture gradient and intensifying poleward moisture transport (e.g., Roe et al. 2015; Stuecker et al. 2018; Armour et al. 2019). In turn, increased poleward moist AHT due to extra-polar cloud feedbacks (blue line in Fig. 7c) acts to warm the Arctic. Hence, the impact of cloud feedbacks on moist AHT partially explains enhanced Arctic warming when cloud changes are included. This additional Arctic warming, driven by increased northward moist AHT, is further amplified by local positive feedbacks in the Arctic. Thus the processes governing cloud-induced changes in AA cannot be studied in isolation, as changes in the local feedbacks, temperature and moisture gradients, and atmospheric heat transport are tightly coupled (e.g., Hwang et al. 2011).

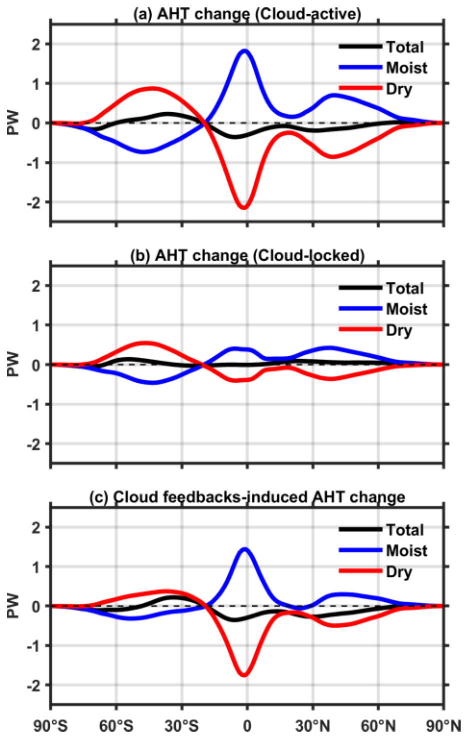

Fig. 7 Changes in atmospheric heat transport (AHT; PW) within E3SM (a) cloud-active simulation and (b) cloud-locked simulation, and (c) the difference in AHT change between cloud-active and cloud-locked simulation: total AHT (black), moist AHT (blue) and dry AHT (red).

So far we have found that extra-polar cloud feedbacks drive AA through two primary mechanisms: (1) positive cloud feedbacks in the tropics and mid-latitudes contribute to local warming, in turn leading to increased poleward moist AHT which then contributes to Arctic warming; (2) the additional Arctic warming is amplified by positive non-cloud feedbacks in the region (such as the surface albedo feedback), altogether making extra-polar cloud feedbacks amplify AA. We also found that changes in atmospheric temperature and moisture owing to cloud changes can modify the strength of local non-cloud feedbacks at all latitudes, which has a small effect on Arctic warming. The combined effect of these mechanisms leads to increased warming contributions from AHT and non-cloud feedbacks to AA when cloud feedbacks are active, as indicated by the shifts in all points between Figs. 3a and 3b. The traditional warming contribution analysis substantially underestimates the role of cloud feedbacks in driving AA since it neglects these interactions. In GCM simulations, these processes are all coupled and act together, making it challenging to disentangle their individual effects.

The above analysis still relies on diagnostic interpretation of the cloud-active and cloud-locking simulations. To further investigate the interaction between cloud feedbacks and AHT, we turn to the moist energy balance model (MEBM), which allows us to isolate the response of AHT to cloud feedbacks while leaving non-cloud feedbacks unchanged. This framework allows us to validate our E3SM-based diagnoses of the role of cloud feedbacks in AA.

f. Moist Energy Balance Model

We employ an MEBM that has been shown to accurately capture changes in zonal-mean temperature and AHT in response to CO_2 forcing as simulated by GCMs (Roe et al. 2015; Siler et al. 2018; Merlis and Henry 2018; Armour et al. 2019; Bonan et al. 2023). MEBMs have been widely used to explore the relative contributions of individual radiative feedbacks to the spatial structure of temperature changes under global warming because they represent the non-local influence of feedbacks via changes in AHT (Hwang and Frierson 2010; Hwang et al. 2011; Roe et al. 2015; Bonan et al. 2018; Beer and Eisenman 2022). In the context of the slab ocean model simulations used in this analysis, in which oceanic heat transport is held fixed, the equilibrium atmospheric energy budget can be expressed as a balance between anomalous top-of-atmosphere radiation (including contributions from radiative forcing and radiative feedbacks) and anomalous AHT divergence:

$$\mathrm{ERF}(x) + \lambda(x)\Delta T(x) = \Delta\nabla \cdot \mathrm{AHT}(x) \tag{4}$$

where ERF is the effective radiative forcing for $4\times CO_2$, λ is the total radiative feedback parameter, ΔT is the surface temperature response to the forcing, $\Delta\nabla \cdot \mathrm{AHT}$ is the anomalous AHT divergence, x is the sine of latitude. We use an MEBM that has been developed and validated in previous studies (Roe et al. 2015; Siler et al. 2018; Bonan et al. 2018; Armour et al. 2019; Beer and Eisenman 2022). In this MEBM, the AHT is approximated as the downgradient diffusion of moist static energy (MSE; h), AHT $= -D\nabla \cdot h$. Hence, the anomalous AHT divergence is given by:

$$\Delta\nabla \cdot \mathrm{AHT}(x) = -D\nabla \cdot \Delta h = -D\frac{d}{dx}\left[(1-x)^2\frac{d\Delta h}{dx}\right] \tag{5}$$

where D is a constant diffusion coefficient and $\nabla \cdot \Delta h$ represents the gradient of the anomalous MSE, where $\Delta h = c_p\Delta T + L_v\Delta q$, c_p is the specific heat of air ($c_p = 1005\, J\, kg^{-1}\, K^{-1}$), L_v is the latent heat of vaporization ($L_v = 2.5 \times 10^6\, J\, kg^{-1}$), ΔT and Δq are the changes in near-surface air temperature and specific humidity, respectively. Δq is calculated using the Clausius–Clapeyron relation and is a function of ΔT (for fixed relative humidity of 80%). We use a diffusion coefficient of $D = 2.6 \times 10^{-4}\, kg\, m^{-2}\, s^{-1}$ taken from previous studies (Hwang and Frierson 2010; Roe et al. 2015; Beer and Eisenman 2022).

Equations (4) and (5) constitute the MEBM that can be used to solve for the surface temperature response pattern $\Delta T(x)$ given specific meridional structures of forcing and feedback. Using the ERF and feedback values (λ, gray line in Fig. 9a) from the E3SM cloud-active simulation, the MEBM predicts a surface warming pattern that closely matches that in the E3SM cloud-active simulation everywhere except in the Southern Ocean (compare blue and black lines in Fig. 8a); the Southern Ocean discrepancy is a known issue of MEBM that remains not fully understood (Siler et al. 2018; Armour et al. 2019; Ge et al. 2024). Similarly, by applying the ERF and feedback values (λ^*, red line in Fig. 9a) from the cloud-locked simulation, the MEBM predicts a surface warming pattern that closely matches that in the E3SM cloud-locked simulation except in the Southern Ocean (compare blue and black lines in Fig. 8b).

The effect of specific feedbacks on the surface temperature response can be examined using a 'feedback locking' approach in the MEBM (Beer and Eisenman 2022). For example, to examine the impact of cloud feedbacks on temperature response, we run the MEBM with the cloud feedbacks parameter subtracted from the total feedback ($\lambda - \lambda_{cloud}$, yellow line in Fig. 9a). The surface temperature response attributed to cloud feedbacks is then obtained by comparing the results of the full MEBM, where all feedbacks are active, with the cloud-locked MEBM, where the cloud feedbacks are excluded. The predicted ΔT with cloud feedback excluded in the MEBM (while the non-cloud feedbacks remain unchanged) shows a similar pattern but a slightly weaker magnitude compared to the E3SM cloud-locked simulation results (compare blue and black lines in Fig. 8c). This suggests that the 'cloud locking' approach in the

MEBM can capture most of the processes simulated in the GCM cloud-locked simulation. However, some differences remain, due to the impact of cloud feedbacks on non-cloud feedbacks (blue line in Fig. 9a) that is not accounted for in the MEBM feedback locking method.

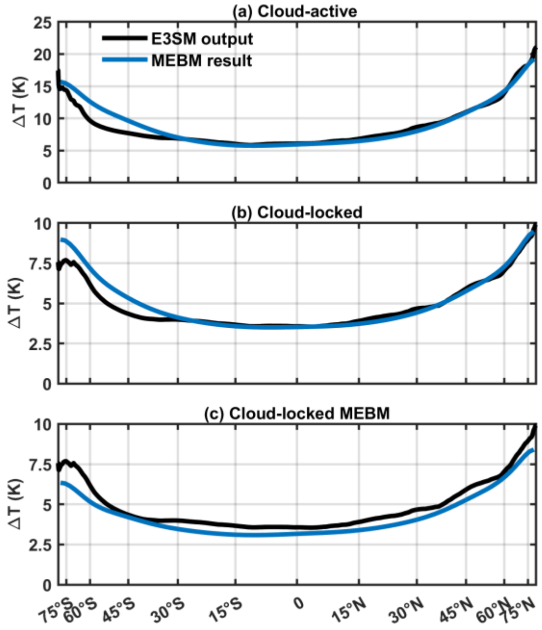

Fig. 8 (a) Predicted surface temperature response in MEBM with total feedbacks from E3SM cloud-active simulation (blue) and surface temperature response in the E3SM cloud-active simulation (black); (b) Same as (a) but for E3SM cloud-locked simulation; (c) Predicted surface temperature response in MEBM with non-cloud feedbacks from E3SM cloud-active simulation (blue) and surface temperature response in the E3SM cloud-locked simulation (black, same as the black line in (b)).

In a comparison of the surface temperature response attributed to cloud feedbacks (i.e., warming contribution of cloud feedbacks) from different approaches, we find that the warming contribution from cloud feedbacks using traditional feedback analysis (ΔT_{cloud1}, green line in Fig. 9b) differs significantly from the contribution estimated using the E3SM cloud lock experiments (ΔT^{*}_{cloud}, black line in Fig. 9b). The primary reason for this discrepancy is that the cloud feedbacks affect surface temperature not only through their direct impact on local radiation (which can be captured by the traditional feedback analysis), but also through their impact on non-local warming through their influence on AHT and on other, non-cloud feedbacks. When the interactions between cloud responses and AHT and other feedbacks are included, the 'cloud locking' method in MEBM (ΔT_{cloud2}, yellow line in Fig. 9b) captures most of the cloud feedbacks-induced temperature responses observed in the E3SM cloud-locked simulation north of 30°S (black line in Fig. 9b). Furthermore, when the influence of cloud feedbacks on the strength of non-cloud feedbacks is considered (where we run the MEBM with λ^{*} taken from E3SM cloud-locked simulation, instead of $(\lambda - \lambda_{cloud})$ from E3SM cloud-active simulation), the MEBM 'cloud locking' method yields a temperature response (ΔT_{cloud3}, red line in Fig. 9b) that aligns more closely with the meridional structure of ΔT from E3SM cloud-locked simulation, except in the Southern Ocean, where the MEBM performs less accurately. The difference between λ^{*} and $\lambda - \lambda_{cloud}$ (blue line in Fig. 9a) and the corresponding difference between ΔT_{cloud3} and ΔT_{cloud2} (blue line in Fig. 9b) are due to the influences of cloud changes on non-cloud feedbacks. These effects lead to cooling at all latitudes, reducing global warming by approximately 14% and Arctic warming by 10%, which acts to slightly enhance AA.

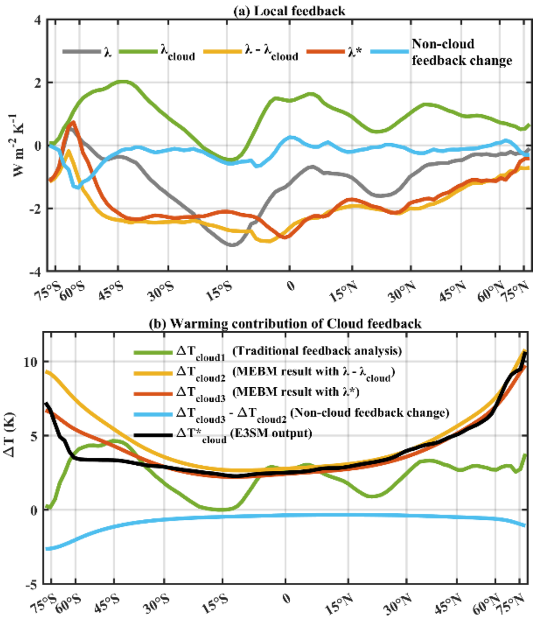

Fig. 9 (a) Total feedback parameter (λ; gray) and cloud feedback parameter (λ_{cloud}; green) from the E3SM cloud-active simulation; the feedback parameter when the cloud feedback is locked but other feedback remain unchanged (λ-λ_{cloud}; yellow), and the feedback parameter from the E3SM cloud-locked simulation (λ*; red), with the difference between the two (i.e., non-cloud feedbacks change caused by cloud changes) also indicated (blue). (b) Warming contribution of cloud feedback derived from different methods: the traditional feedback analysis (ΔT_{cloud1}; green); MEBM feedback locking analysis (ΔT_{cloud2}; yellow); modified MEBM feedback locking analysis (ΔT_{cloud3}; red); the difference between two MEBM results (ΔT_{cloud3}- ΔT_{cloud2}; blue) ; E3SM cloud locking method (ΔT^{*}_{cloud}; black).

To further quantify the contribution of interactions between cloud feedbacks and AHT, as well as between cloud feedbacks and other feedbacks to AA, we decompose the warming contribution of cloud feedbacks that is derived from MEBM (both ΔT_{cloud2} and ΔT_{cloud3}) into three components (following Beer and Eisenman 2022), each owning to: (1) cloud feedbacks themselves using traditional feedback analysis; (2) interactions between the cloud feedbacks induced warming and other climate feedbacks (referred to as feedback interactions); and (3) interactions between the cloud feedbacks and AHT (referred to as AHT interactions). These three contributions can be calculated as follows:

$$\Delta T_{cloud2} = \Delta T_{cloud1} + \frac{(\lambda-\lambda_{cloud})\Delta T_{cloud2}}{-\lambda_p} + \frac{\Delta\nabla\cdot\mathrm{AHT} - \Delta\nabla\cdot\mathrm{AHT}_{-cloud2}}{-\lambda_p} \qquad (6)$$

$$\Delta T_{cloud3} = \Delta T_{cloud1} + \frac{\lambda^{*}\Delta T_{cloud3}}{-\lambda_p} + \frac{\Delta\nabla\cdot\mathrm{AHT} - \Delta\nabla\cdot\mathrm{AHT}_{-cloud3}}{-\lambda_p} \qquad (7)$$

In addition, the contributions of AHT interactions can be partitioned into moist and dry components following Siler et al. (2018) and Armour et al. (2019). Equations (6) and (7) represent the decompositions when the effect of cloud feedbacks on non-cloud feedbacks is not considered and when it is considered, respectively. The difference between these two decompositions in (6) and (7) gives the warming contribution from changes in non-cloud feedbacks caused by cloud feedbacks through the three processes outlined above.

As shown previously, the warming contribution of cloud feedbacks is slightly positive to AA in the traditional feedback analysis (blue bars in Fig. 10). However, this alone is insufficient to explain the significant influence of cloud feedbacks on AA. The dominant influence of cloud feedbacks on AA arises from their interaction with other feedbacks and interaction with the moist AHT (green and yellow bars in Fig. 10), while the cloud-induced interaction with dry AHT warms the tropics but cools the Arctic (red bars in Fig. 10). Moreover, the contrast in warming contributions between Arctic and tropical regions show little variation when the effects of cloud feedbacks on non-cloud feedback parameters are considered (not shown), indicating that the contribution of changes in non-cloud feedback parameters to AA is relatively small.

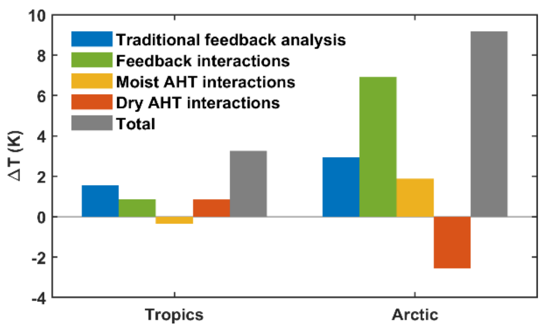

Fig. 10 Decomposition of warming contribution of cloud feedback (Total) into contributions from the individual contribution of the cloud feedbacks alone, interactions with other feedbacks, and interactions with AHT (both its moist and dry components) in tropics (30°S–30°N) and polar (60°N–90°N).

4. Summary and discussion

This study investigates the role of cloud feedback in Arctic amplification (AA) using cloud locking techniques within the Energy Exascale Earth System Model (E3SM) and a moist energy balance model (MEBM). By comparing the climate response in simulations with and without active cloud changes in response to 4×CO_2, we find that cloud feedbacks substantially enhance AA under greenhouse gas forcing. This contrasts with the results of traditional feedback analyses, which suggest that cloud feedbacks contribute minimally or negatively to AA.

The role of cloud feedbacks in driving AA is substantially underestimated in the traditional warming contribution analysis because it only captures the direct impact of cloud feedbacks on local radiation. In contrast, the strong positive contribution of cloud feedbacks to AA is achieved through indirect mechanisms. We identify two key mechanisms through which cloud feedbacks contribute indirectly to AA: (1) Positive cloud feedbacks in the tropics increase poleward moist atmospheric heat transport (AHT), which amplifies Arctic warming. This process suggests that tropical cloud responses indirectly affect the Arctic by modifying global energy transport. (2) As Arctic warming intensifies, the additional Arctic warming further amplifies the warming contribution of other positive non-cloud feedbacks in the region, such as the surface albedo feedback, further enhancing AA. In addition, we found that changes in atmospheric warming structure caused by cloud feedbacks can alter the strength of non-cloud feedbacks. Specifically, the water vapor feedback becomes more positive in the tropics, while the surface albedo feedback becomes less positive in the Arctic when clouds are active. However, the changes in global non-cloud feedbacks are very small and have only a minor effect on Arctic warming.

The combined effect of these mechanisms results in the positive contribution of cloud feedbacks to AA. However, these processes are highly coupled and operate simultaneously, making it difficult to isolate their individual impacts in global climate model (GCM) simulations. To address this, we employed a moist energy balance model (MEBM) to quantify the contributions of each mechanism separately. Results from the MEBM support the interpretation of the E3SM cloud locking simulations. Namely, that the dominant influence of cloud feedbacks on AA arises from their influence on AHT and interactions with other Arctic regional feedbacks. Moreover, the contribution of changes in global non-cloud feedbacks slightly enhances the AA, but this effect is secondary.

In summary, the contribution of tropical and mid-latitude cloud feedbacks to AA is largely indirect. They act to intensify AA primarily by amplifying the warming impact of other feedbacks rather than through a direct warming effect. In essence, tropical-amplified positive cloud feedbacks drive stronger global warming, increasing poleward moist AHT which further amplifies the warming effects of other polar-amplified positive feedbacks in the Arctic—such as the lapse-rate and surface-albedo feedbacks. An implication of this result is that a larger portion of the uncertainty in AA may stem from the remote influence of uncertainties in extra-polar cloud feedbacks than has previously been appreciated.

This indirect mechanism suggests that the cloud feedbacks alone may not significantly contribute to AA in the absence of these polar-amplified positive feedbacks. This speculation is verified by locking the cloud feedback in a MEBM that includes only the Planck feedback and cloud feedbacks; in this scenario, we find that suppressing cloud feedbacks causes nearly uniform global cooling but results in almost no change in AA when conducting the cloud-locked simulation without other feedbacks present (Fig. A4).

This indirect mechanism identified here by which extra-polar feedbacks can contribute to AA through their effect on AHT and interaction with other positive feedbacks in the Arctic likely applies to other feedbacks as well. For instance, Beer and Eisenman (2020) identified the water-vapor feedback (strongly positive in the tropics) as a primary driver of AA using the feedback locking method in MEBM. Motivated by previous studies that examined how local responses depend on nonlocal climate processes using the MEBM (Beer and Eisenman 2020; David et al. 2018), our conclusions from both E3SM simulations and the MEBM show strong agreement with these earlier works.

The discrepancies between the conclusions of traditional feedback analysis methods and the cloud locking approach arises from whether the method accounts for indirect influences of feedbacks on AHT and interactions with other feedbacks. Traditional feedback analyses (i.e., “warming contribution” attributions of AA) often treat cloud feedbacks in isolation, resulting in an incomplete understanding of their role in AA. In contrast, the cloud locking method effectively captures these interactions, demonstrating that extra-polar cloud feedbacks indirectly enhance AA by influencing energy transport and amplifying the warming effect of non-cloud feedbacks.

Acknowledgments.

We thank Angeline Pendergrass for providing calculation and tools for radiative feedback kernels, Aaron Donohoe for helping with the kernel analysis and validation. We also thank Yi Qin for providing the E3SM fixed-SST simulation data. Q.L., W.C., and J.Z. were supported by the U.S. Department of Energy, Office of Science, Office of Biological and Environmental Research (BER) Regional and Global Model Analysis (RGMA) program under Award Number DE-SC0022080. B.H. and O.G were supported by the US Department of Energy (DOE) Office of Science Biological and Environmental Research (BER) as part of the Regional and Global Model Analysis program area through the Water Cycle and Climate Extremes Modeling (WACCEM) and High Latitude Application and Testing of Earth System Models (HiLAT-RASM) Scientific Focus Areas. The Pacific Northwest National Laboratory (PNNL) is operated for DOE by Battelle Memorial Institute (contract no. DE-AC05-76RLO1830). K.C.A. was supported by National Science Foundation Award AGS-1752796 and a Calvin Professorship in Oceanography. L.T. was supported by the National Oceanic and Atmospheric Administration Climate Program Office, Climate Variability and Predictability Program under Award Number NA22OAR4310596-T1-01. Y. L. was supported by the National Natural Science Foundation of China (NSFC; 42230405). This publication is partially funded by the Cooperative Institute for Climate, Ocean, & Ecosystem Studies (CICOES) under NOAA Cooperative Agreement NA20OAR4320271, Contribution No. 2024-1427. This publication is the NOAA/PMEL contribution number 5697. This research was performed using resources of the National Energy Research Scientific Computing Center, a DOE Office of Science User Facility supported by the Office of Science of the US Department of Energy (contract no. DE-AC02-05CH11231).

Data Availability Statement.

The E3SM cloud-active and cloud-locked simulation data used in this study are available from the corresponding authors upon request. The source code builds off of E3SM version 2.0 (DOI: 10.11578/E3SM/dc.20210927.1) including cloud locking and slab ocean model modifications taken from a fork of the model available at https://github.com/beharrop/E3SM and https://github.com/ogaruba/E3SM/tree/ogaruba/E3SMv2_slab. The CAM5 radiative feedback kernels can be found at: https://zenodo.org/record/997902. The E3SM fixed-SST simulation data is from Qin et al. (2024).

APPENDIX

Appendix Figures

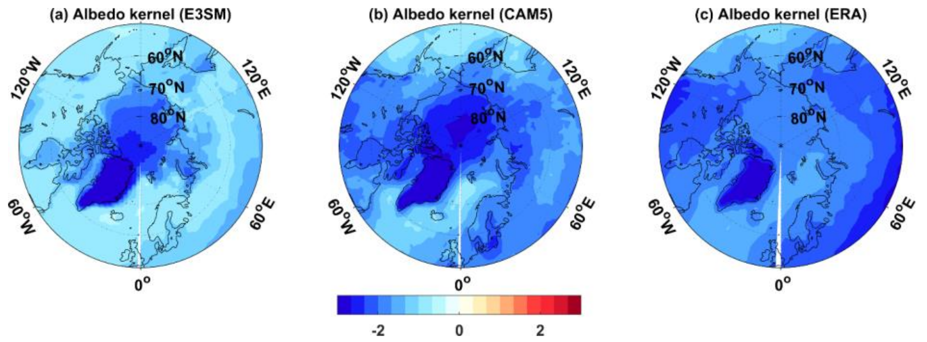

Fig. A1 The surface albedo kernel (W m^{-2} $\%^{-1}$) derived from (a) the climatological radiative fields in E3SM model using idealized isotropic radiation model, (b) CESM1-CAM5 model (Pendergrass et al. 2018) and (c) ERAi data (Huang et al. 2017).

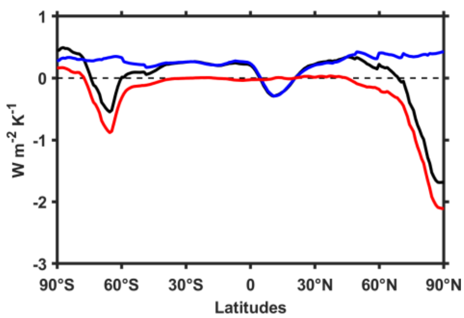

Fig. A2 The error in the clear-sky feedback decomposition using the kernel method.

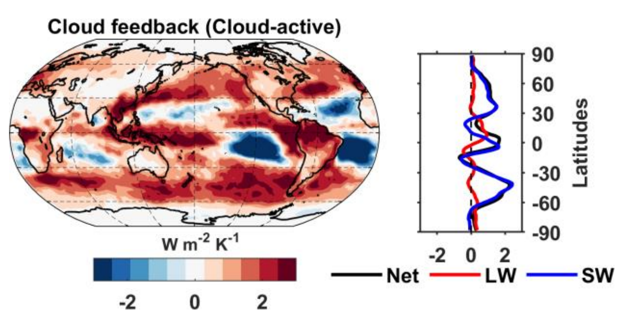

Fig. A3 The cloud feedbacks in E3SM cloud-active simulation derived using the Cloud Radiative Kernel method (Zelinka et al. 2012). The right-side panel is the zonal mean net cloud feedback (black) and its longwave (LW, red) and shortwave (SW, blue) components.

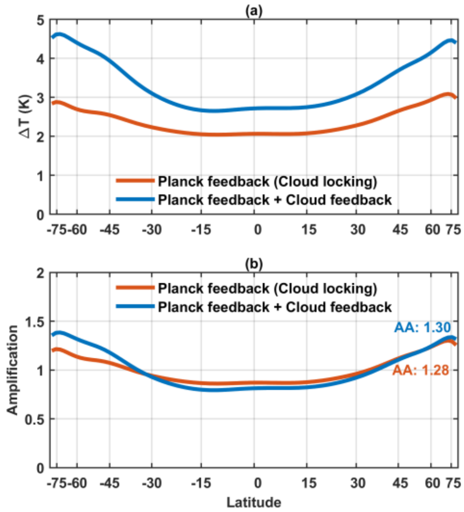

Fig. A4 Predicted surface temperature response in MEBM with Planck feedback (red) and Planck feedback plus cloud feedbacks (blue) from E3SM cloud-active simulation; (b) Predicted amplification (zonal-mean surface warming normalized by global-mean surface warming) in MEBM with Planck feedback (red) and Planck feedback plus cloud feedbacks (blue). The numbers in (b) are the AA factor in MEBM with Planck feedback (red) and Planck feedback plus cloud feedbacks (blue).

REFERENCES

Armour, K. C., C. M. Bitz, and G. H. Roe, 2013: Time-varying climate sensitivity from regional feedbacks. *J. Climate*, **26**, 4518–4534.

——, N. Siler, A. Donohoe, and G. Roe, 2019: Meridional atmospheric heat transport constrained by energetics and mediated by large-scale diffusion. *J. Climate*, **32**, 3655–3680.

Beer, E., and I. Eisenman, 2022: Revisiting the role of the water vapor and lapse rate feedbacks in the Arctic amplification of climate change. *J. Climate*, **35**, 2975–2988.

Boeke, R. C., and P. C. Taylor, 2016: Evaluation of the Arctic surface radiation budget in CMIP5 models. *J. Geophys. Res.*, **121**, 8525–8548.

Bonan, D. B., K. C. Armour, G. H. Roe, N. Siler, and N. Feldl, 2018: Sources of uncertainty in the meridional pattern of climate change. *Geophys. Res. Lett.*, **45**(17), 9131–9140.

——, N. Siler, G. H. Roe, and K. C. Armour, 2023: Energetic constraints on the pattern of changes to the hydrological cycle under global warming. *J. Climate*, **36**(10), 3499–3522.

Caldwell, P. M., A. Mametjanov, Q. Tang, L. P. Van Roekel, J.-C. Golaz, W. Lin, D. C. Bader, and Coauthors, 2019: The DOE E3SM Coupled Model Version 1: Description and Results at High Resolution. *J. Adv. Model. Earth Syst.*, **11**, 4095–4146, https://doi.org/10.1029/2019MS001870.

——, M. D. Zelinka, K. E. Taylor, and K. Marvel, 2016: Quantifying the sources of intermodel spread in equilibrium climate sensitivity. *J. Climate*, **29**, 513–524, https://doi.org/10.1175/JCLI-D-15-0352.1.

Charlock, T. P., and V. Ramanathan, 1985: The albedo field and cloud radiative forcing produced by a general circulation model with internally generated cloud optics. *J. Atmos. Sci.*, **42**, 1408–1429.

Collins, M., R. Knutti, J. Arblaster, J.-L. Dufresne, T. Fichefet, P. Friedlingstein, and Coauthors, 2013: Long-term climate change: Projections, commitments and irreversibility. In T. F. Stocker et al. (Eds.), *Climate Change 2013: The Physical Science Basis*. Contribution of Working Group I to the Fifth Assessment Report of the Intergovernmental Panel on Climate Change (pp. 1029–1136). Cambridge University Press.

Constable, A.J., S. Harper, J. Dawson, K. Holsman, T. Mustonen, D. Piepenburg, and B. Rost, 2022: Cross-Chapter Paper 6: Polar Regions. In: Climate Change 2022: Impacts, Adaptation and Vulnerability. Contribution of Working Group II to the Sixth Assessment Report of the Intergovernmental Panel on Climate Change [H.-O. Pörtner, D.C. Roberts, M. Tignor, E.S. Poloczanska, K. Mintenbeck, A. Alegría, M. Craig, S. Langsdorf, S. Löschke, V. Möller, A. Okem, B. Rama (eds.)]. Cambridge University Press, Cambridge, UK and New York, NY, USA, pp. 2319–2368, doi:10.1017/9781009325844.023.

Coulbury, C., and I. Tan, 2024: Top of the atmosphere shortwave Arctic cloud feedbacks: A comparison of diagnostic methods. *Geophys. Res. Lett.*, **51**, e2023GL107780, https://doi.org/10.1029/2023GL107780.

Donohoe, A., E. Blanchard-Wrigglesworth, A. Schweiger, and P. J. Rasch, 2020a: The effect of atmospheric transmissivity on model and observational estimates of the sea ice albedo feedback. *J. Climate*, **33**, 5743–5765.

——, K. C. Armour, G. H. Roe, D. S. Battisti, and L. Hahn, 2020b: The partitioning of meridional heat transport from the Last Glacial Maximum to CO_2 quadrupling in coupled climate models. *J. Climate*, **33**(10), 4141–4165, https://doi.org/10.1175/JCLI-D-19-0797.1.

Feldl, N., and T. M. Merlis, 2021: Polar amplification in idealized climates: The role of ice, moisture, and seasons. *Geophys. Res. Lett.*, **48**(17), e2021GL094130.

Forster, P., T. Storelvmo, K. Armour, W. Collins, J. Dufresne, D. Frame, et al., 2021: The Earth's energy budget, climate feedbacks, and climate sensitivity. *Climate Change 2021: The Physical Science Basis*, V. Masson-Delmotte, P. Zhai, A. Pirani, S. L. Connors, C. Péan, S. Berger, et al., Eds., Contribution of Working Group I to the Sixth Assessment Report of the Intergovernmental Panel on Climate Change, Cambridge University Press.

Garuba, O., P. J. Rasch, L. R. Leung, H. Wang, S. Hagos, and B. Singh, 2024: Slab ocean component of the energy exascale Earth system model (E3SM): Development, evaluation, and application to understanding Earth system sensitivity. *J. Adv. Model. Earth Syst.*, **16**, e2023MS003910, https://doi.org/10.1029/2023MS003910.

Golaz, J.-C., L. P. Van Roekel, X. Zheng, A. F. Roberts, J. D. Wolfe, W. Lin, and Coauthors, 2022: The DOE E3SM model version 2: Overview of the physical model and initial model evaluation. *J. Adv. Model. Earth Syst.*, **14**(12), e2022MS003156, https://doi.org/10.1029/2022MS003156.

González-Herrero, S., M. Lemus-Canovas, and P. Pereira, 2024: Climate change in cold regions. Science *of The Total Environment*, **933**, 173127, https://doi.org/10.1016/j.scitotenv.2024.173127.

Goosse, H., J. E. Kay, K. C. Armour, A. Bodas-Salcedo, H. Chepfer, D. Docquier, and Coauthors, 2018: Quantifying climate feedbacks in polar regions. *Nat. Commun.*, **9**, 1919, https://doi.org/10.1038/s41467-018-04173-0.

Grise, K. M., B. Medeiros, J. J. Benedict, and J. G. Olson, 2019: Investigating the influence of cloud radiative effects on the extratropical storm tracks. *Geophys. Res. Lett.*, **46**(13), 7700–7707.

Hahn, L. C., K. C. Armour, M. D. Zelinka, C. M. Bitz, and A. Donohoe, 2021: Contributions to polar amplification in CMIP5 and CMIP6 models. *Front. Earth Sci.*, **9**, 710036.

Harrop, B. E., J. Lu, L. R. Leung, W. K. M. Lau, K.-M. Kim, B. Medeiros, and Coauthors, 2024: An overview of cloud–radiation denial experiments for the Energy Exascale Earth System Model version 1. *Geosci. Model Dev.*, **17**, 3111–3135.

Holland, M. M., and C. M. Bitz, 2003: Polar amplification of climate change in coupled models. *Climate Dyn.*, **21**(3), 221–232.

Huang, Y., H. Huang, and A. Shakirova, 2021: The nonlinear radiative feedback effects in the Arctic warming. *Front. Earth Sci.*, **9**, 693779.

——,, Y. Xia, and X. X. Tan, 2017: On the pattern of CO_2 radiative forcing and poleward energy transport. *J. Geophys. Res. Atmos.*, **122**, 10,578–10,593. https://doi.org/10.1002/2017JD027221

Huang, H., and Y. Huang, 2021: Nonlinear coupling between longwave radiative climate feedbacks. *J. Geophys. Res. Atmos.*, **126**, e2020JD033995, https://doi.org/10.1029/2020JD033995.

Hwang, Y.-T., and D. Frierson, 2010: Increasing atmospheric poleward energy transport with global warming. *Geophys. Res. Lett.*, **37**, L24807, https://doi.org/10.1029/2010GL045440.

——, ——, and J. Kay, 2011: Coupling between Arctic feedbacks and changes in poleward energy transport. *Geophys. Res. Lett.*, **38**, L17704, https://doi.org/10.1029/2011GL048546.

Kato, S., Rose, F. G., Rutan, D. A., Thorsen, T. J., Loeb, N. G., Doelling, D. R., et al. (2018). Surface irradiances of edition 4.0 Clouds and the Earth's Radiant Energy System (CERES) Energy Balanced and Filled (EBAF) data product. *J. Climate*, **31**(11), 4501–4527.

Kay, J. E., & Gettelman, A. (2009). Cloud influence on and response to seasonal Arctic sea ice loss. *J. Geophys. Res.*, *114*, D18204. https://doi.org/10.1029/2009JD011773

Kato, S., F. G. Rose, D. A. Rutan, T. J. Thorsen, N. G. Loeb, D. R. Doelling, and Coauthors, 2018: Surface irradiances of edition 4.0 Clouds and the Earth's Radiant Energy System (CERES) Energy Balanced and Filled (EBAF) data product. *J. Climate*, **31**(11), 4501–4527.

Kay, J. E., and A. Gettelman, 2009: Cloud influence on and response to seasonal Arctic sea ice loss. *J.* Geophys. *Res.*, **114**, D18204, https://doi.org/10.1029/2009JD011773.

Manabe, S., and R. J. Stouffer, 1980: Sensitivity of a global climate model to an increase of CO_2 concentration in the atmosphere. *J. Geophys. Res. Oceans*, **85**(C10), 5529–5554.

Mauritsen, T., R. G. Graversen, D. Klocke, P. L. Langen, B. Stevens, and L. Tomassini, 2013: Climate feedback efficiency and synergy. *Climate Dyn.*, **41**(9–10), 2539–2554, https://doi.org/10.1007/s00382-013-1808-7.

Merlis, T. M., and M. Henry, 2018: Simple estimates of polar amplification in moist diffusive energy balance models. *J. Climate*, **31**(15), 5811–5824. https://doi.org/10.1175/JCLI-D-17-0578.1

Middlemas, E. A., J. E. Kay, B. M. Medeiros, and D. L. Hartmann, 2020: Quantifying the influence of cloud radiative feedbacks on Arctic surface warming using cloud locking in an Earth system model. *Geophys. Res. Lett.*, **48**, e2020GL091890, https://doi.org/10.1029/2020GL091890.

Pendergrass, A. G., A. Conley, and F. M. Vitt, 2018: Surface and top-of-atmosphere radiative feedback kernels for CESM-CAM5. *Earth Syst. Data*, **8**.

Petersen, M. R., X. S. Asay-Davis, A. S. Berres, Q. Chen, N. Feige, M. J. Hoffman, and Coauthors, 2019: An evaluation of the ocean and sea ice climate of E3SM using MPAs and interannual core-II forcing. *J. Adv. Model. Earth Syst.*, **11**(5), 1438–1458, https://doi.org/10.1029/2018MS001373.

Pithan, F., and T. Mauritsen, 2014: Arctic amplification dominated by temperature feedbacks in contemporary climate models. *Nat. Geosci.*, **7**, 181–184.

Previdi, M., K. L. Smith, and L. M. Polvani, 2021: Arctic amplification of climate change: A review of underlying mechanisms. *Environ. Res. Lett.*, **16**, 093003.

Qin, Y., X. Zheng, S. A. Klein, M. D. Zelinka, P.-L. Ma, J.-C. Golaz, and S. Xie, 2024: Causes of reduced climate sensitivity in E3SM from version 1 to version 2. *J. Adv. Model. Earth Syst.*, **16**, e2023MS003875, https://doi.org/10.1029/2023MS003875.

Randall, D., and Coauthors, 1998: Status of and outlook for large-scale modeling of atmosphere–ice–ocean interactions in the Arctic. *Bull. Amer. Meteor. Soc.*, **79**, 197–219.

Rasch, P., S. Xie, P.-L. Ma, W. Lin, H. Wang, Q. Tang, and Coauthors, 2019: An overview of the atmospheric component of the energy exascale Earth system model. *J. Adv. Model. Earth Syst.*, **11**(8), 2377–2411, https://doi.org/10.1029/2019MS001629.

Rayner, N. A., D. E. Parker, E. B. Horton, ,C. K. Folland, L. V. Alexander, D. P. Rowell, E. C. Kent, and A. Kaplan, 2003: Global analyses of sea surface temperature, sea ice, and night marine air temperature since the late nineteenth century. *J. Geophys. Res. Atmos.*, **108**(D14), 4407. https://doi.org/10.1029/2002JD002670

Roe, G. H., N. Feldl, K. C. Armour, Y.-T. Hwang, and D. M. W. Frierson, 2015: The remote impacts of climate feedbacks on regional climate predictability. *Nat. Geosci.*, **8**, 135–139.

Screen, J. A., and I. Simmonds, 2010: The central role of diminishing sea ice in recent Arctic temperature amplification. *Nature*, **464**, 1334–1337, https://doi.org/10.1038/nature09051.

Serreze, M., A. Barrett, J. Stroeve, D. Kindig, and M. Holland, 2009: The emergence of surface-based Arctic amplification. *Cryosphere*, **3**(1), 11–19.

Shell, K. M., J. T. Kiehl, and C. A. Shields, 2008: Using the radiative kernel technique to calculate climate feedbacks in NCAR's Community Atmospheric Model. *J. Climate*, **21**(10), 2269–2282.

Shupe, M. D., and J. M. Intrieri, 2004: Cloud radiative forcing of the Arctic surface: The influence of cloud properties, surface albedo, and solar zenith angle. *J. Climate*, **17**(3), 616–628.

Siler, N., G. H. Roe, and K. C. Armour, 2018: Insights into the zonal-mean response of the hydrologic cycle to global warming from a diffusive energy balance model. *J. Climate*, **31**, 7481–7493.

Singh, H., P. Rasch, and B. Rose, 2017: Increased ocean heat convergence into the high latitudes with CO2_22 doubling enhances polar-amplified warming. *Geophys. Res. Lett.*, **44**(20), 10–583.

Soden, B. J., I. M. Held, R. Colman, K. M. Shell, J. T. Kiehl, and C. A. Shields, 2008: Quantifying climate feedbacks using radiative kernels. *J. Climate*, **21**(14), 3504–3520.

Stuecker, M. F., and Coauthors, 2018: Polar amplification dominated by local forcing and feedbacks. *Nat. Climate Change*, **8**, 10761, https://doi.org/10.1038/s41558-018-0339-y.

Taylor, P. C., R. C. Boeke, L. N. Boisvert, N. Feldl, M. Henry, Y. Huang, et al., 2021: Process drivers, inter-model spread, and the path forward: A review of amplified Arctic warming. *Front. Earth Sci.*, **9**.

Vavrus, S., 2004: The impact of cloud feedbacks on Arctic climate under greenhouse forcing. *J.* Climate, **17**(3), 603–615.

Voigt, A., and T. Shaw, 2015: Circulation response to warming shaped by radiative changes of clouds and water vapour. *Nat. Geosci.*, **8**, 102–106.

Zelinka, M. D., T. A. Myers, D. T. McCoy, S. Po-Chedley, P. M. Caldwell, P. Ceppi, S. A. Klein, and K. E. Taylor, 2020: Causes of higher climate sensitivity in CMIP6 models. *Geophys. Res. Lett.*, **47**, e2019GL085782, https://doi.org/10.1029/2019GL085782.

——, S. A. Klein, and D. L. Hartmann, 2012: Computing and Partitioning Cloud Feedbacks Using Cloud Property Histograms. Part I: Cloud Radiative Kernels. *J. Climate*, **25**, 3715–3735, https://doi.org/10.1175/JCLI-D-11-00248.1.

Zhu, T., Y. Huang, and H. Wei, 2019: Estimating climate feedbacks using a neural network. *J. Geophys. Res.* Atmos., **124**(6), 3246–3258.